Article

Journal of
Nanoscience and Nanotechnology
Vol. 18, 7405–7413, 2018
www.aspbs.com/jnn

Efficient Solar Light Driven Photocatalytic Degradation of Congo Red Dye on CdS Nanostructures Derived from Single Source Precursor

Jamal Abdul Nasir[1], Shaheen Gul[1], Azam Khan[1], Zawar Hussain Shah[1], Abrar Ahmad[1], Zulfiqar[2], Rajwali Khan[2], Zhongxin Liu[3], Wei Chen[4], Dan-Jae Lin[5], and Zia-ur-Rehman[1,*]

[1]*Department of Chemistry, Quaid-i-Azam University Islamabad-45320, Pakistan*
[2]*Department of Physics, Abdul Wali Khan University Mardan 23200, KPK, Pakistan*
[3]*Key Laboratory of Advanced Materials of Tropical Island Resources, Ministry of Education; State Key Lab of Marine Resource Utilization in South China Sea, Hainan University, Haikou 570228, China*
[4]*Department of Physics, University of Texas at Arlington, Arlington, Texas 76019, USA*
[5]*Department of Dental Hygiene, China Medical University, Taichung, Taiwan 40402, ROC*

This article presents a facile synthesis of cadmium sulfide nanorods (CdS-NR) and nanospheres (CdS-NS) using cadmium(II) dithiocarbamate as a precursor in the presence of two different thermalizing solvents {ethylenediamine (en) and octylamine (OA)}. The as-synthesized CdS-NR and CdS-NS were characterized by powder X-ray diffraction (PXRD), transmission electron microscopy (TEM), selected area electron diffraction technique (SAED), fourier transmission infrared spectroscopy (FTIR), energy dispersive X-ray spectroscopy (EDS), UV-visible spectroscopy, steady-state and time resolved photoluminesce (PL). TEM analysis has confirmed the formation of nanorods and nanospheres in the presence of en and OA, respectively. The *in situ* generated different capping ligands, as confirmed by FT-IR analysis, may be responsible for variation in morphology. The XRD results revealed hexagonal (nanorods) and cubic mixed hexagonal phase (nanospheres). Owing to band gapes (UV-Vis) in the visible region, both these nanostructures (nanorods and nanospheres) were tested as a solar light drive photocatalyst for the degradation of Congo red (CR). The results indicated that CdS-NR exhibit better catalytic efficiency ($K_{app} = 0.366$ min^{-1}) toward CR degradation as compared to CdS-NS ($K_{app} = 0.299$ min^{-1}). The better photocatalytic activity of nanorods can be attributed to the anisotropically grown structure which infers longer electron hole recombination time as revealed by the time resolved PL.

Keywords: CdS, Nanorods, Nanospheres, Mechanism, Photocatalysis.

1. INTRODUCTION

Synthetic dyes are widely used in various branches of textile industry.[1,2] Study survey estimated that 1–15% of the synthetic dyes are lost during dying and finishing processes i.e., 1–2% during production and 10–12% during use. The lost and release of these dyes into the wastewaters is a serious problem to aquatic biological processes.[3–5] To mitigate this, a wide range of methodologies have been developed such as ozone treatment,[6] adsorption,[7] filtration,[8] solvent extraction[9] and biodegradation.[10] However, formation of secondary waste and required supporting materials are the problems associated with aforesaid techniques.[11] In recent years, research has been focused on the development of efficient photocatalyst to harvest the abundant solar energy for generating environment friendly fuels (H_2) and remove organic pollutants to meet highly mounting energy crisis and ensure safe and clean environment. In addition, environmental friendliness photocatalytic dye degradation processes is considered a cost-effective approach to degrade organic pollutants.[12]

In this context various nanostructured semiconductors have been investigated as photocatalysts[13] such as nitrides,[14] oxides,[15–20] oxy-nitrides[21–23] and sulfides[24–27] to address the mentioned problem of great concern. TiO_2 is

*Author to whom correspondence should be addressed.

considered the most durable photocatalyst for the remediation of environmental pollution.[28] However, TiO_2 has band gap of about 3.0 to 3.2 eV and can only be activated by UV light with a wavelength below 400 nm. This hamper its uses as photocatalyst, because the solar spectrum contain only 3–4% of UV light.[29] So it is direly needed to develop semiconductor that can harvest the bounteous visible light (43%) of the solar spectrum. Among various type of the semiconductors, metal sulfide nanocatalysts are promising candidates for organic dyes degradation due to their powerful oxidation capability.[30, 31] CdS, a visible light driven photocatalyst is considered as a promising material for this purpose because of its suitable band gap (2.42 eV), good photochemical and photocatalytic properties.[12] However, the fast recombination process hinders its effective use. To enhance the photocatalytic efficiency of CdS photocatalyst some efforts have been made such as controlling the morphology, particle size and crystallinity.[32, 33] These features directly influence the position of band gap structure, transport of the photogenerated carriers and their separation. So far, numerous morphologies of CdS nanostructures such as nanosheets, nanorods,[34] micro/nano leaves,[35] hollow microrods,[36] nanosteps,[37] microtower,[38] and multi-armed nanorods[39] have been synthesized by different techniques and evaluated for photocatalysis.

In this work, Cd(II) dithiocarbamate was synthesized and used as single source precursor for the synthesis of cadmium sulfide NPs by thermolysing it in ethylenediamine (en) and octylamine (OA) as schematically shown in Scheme 1 and the photocatalytic efficiency of the obtained nanostructures was tested towards CR degradation under direct sunlight as a model reaction. Different parameters of the photocatalytic reaction were investigated and their kinetic behavior was assessed.

2. EXPERIMENTAL DETAILS

2.1. Materials

Diethylamine and CS_2 were purchased from Fluka. Congo red (M.W = 696.67, $C_{32}H_{24}N_6O_6S_2Na_2$) was purchased from Merck. Methanol, ethylenediamine, octylamine and all other solvents and metal salts of analytical grade were purchased from Sigma Aldrich and used without further purification.

2.2. Synthesis of Ligand Salt, Cd(II) Dithiocarbamates Complex and CdS Nanostructures

The ligand, Sodium diethylcarbamodithioate ($C_5H_{10}NS_2Na$), was synthesized as described in our previous report.[40] For the synthesis of Cd(II) complex, Sodium diethylcarbamodithioate (171 g/mol, 1 g, 0.0058 moles), was dissolved in methanol and added dropwise to methanolic solution of cadmium nitrate tetrahydrate ($Cd(NO_3)_2 \cdot 4H_2O$, 236 g/mol, 1.36 g, 0.0058 moles) with constant stirring, which was continued for four hours. The resulted cadmium complex $[Cd(C_5H_{10}NS_2)_2]$ was filtered off, washed with methanol and dried under IR lamp. The as-synthesized complex was decomposed in two different solvents i.e., ethylenediamine (en) and octylamine (OA) to generate CdS NR and CdS-NS respectively. Appropriate amount of the precursor complex was mixed with thermolysisng solvent (en, OA) in a two neck flask. The mixture was slowly heated up to the boiling point of en (~120 °C) and OA (~175 °C) respectively, with constant stirring. In each experiment the yellow precepitate of CdS appeared at the boiling point of respective thermolysing solvent, which was filtered, washed two to three times with methanol and then dried in oven at 60 °C for four hours.

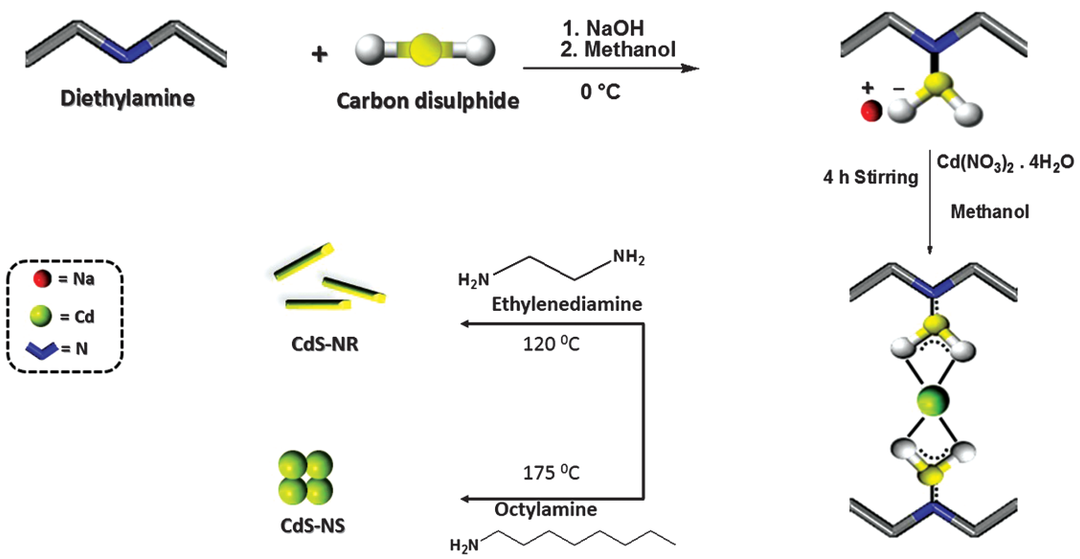

Scheme 1. Synthesis of ligand, complex and CdS nanostructures.

2.3. Photocatalysis

The CdS nanorods and nanosphers mediated photocatalytic degradation of Congo red dye was investigated under direct sunlight in sunny days in May 2017 between 9 to 11:30 am (GPS coordinates N = 33°43′5″, E = 73°3′38″). Pyrex glass vessel of 100 mL capacity was used for performing the photocatalytic experiments. Typically 20 mg of CdS-NR and CdS-NS were uniformly and separately dispersed in 100 mL of freshly prepared Congo Red (CR) aqueous solution (10 mg/L). Before exposure to sunlight the suspension was kept in dark with stirring for 30 minutes to establish the adsorption equilibrium between dye and photocatalyst and then exposed to direct sunlight with stirring. To monitor the degradation of dye, 2 mL of the sample was taken out with the interval of three minutes and centrifuged to separate the catalyst and then dye in the supernatant was analyzed by UV-visible absorption spectroscopy.

2.4. Characterization

The structure of ligand and complex was confirmed by ^{13}C and ^{1}H using Bruker AC 300 MHz-FT-NMR spectrometer. CHNS analyzer 932 LECO (USA) was used for the determination of elemental analysis. The instrument PAN analytical X'Pert powder was used for X-ray diffraction (PXRD) analysis. The instrument has a Cu K$\acute{\alpha}$ radiation wavelength ($\lambda = 1.5418$ Å) and the values of 2θ were recorded from 10° to 80°. To take the UV-visible spectra of CdS-NR and CdS-NS, Shimadzu double beam Spectrophotometer 1800 was used with UV-visible analyze lamp SN: 500412 to provide UV source and its wavelength was adjusted at 250 nm to 800 nm. Bio-Rad Excalibur FTS model 3000 MX in the frequency range of 4000–400 cm^{-1} was used to record the infra-red absorption spectrum of CdS-NR and CdS-NS. The determination of % composition of synthesized NPs was performed on the Energy Dispersive X-ray (EDX) analyzer JED-2300/2300F. Transmission Electron Microscopy (TEM) images were taken on JEOL 2010 microscope with an accelerating voltage of 200 kV. Time-correlated single photon counting (TCSPC) setup (FluoTime300, PicoQuant GmbH) was used for the determination of time-resolved and Steady-state Photoluminescence (PL) measurements.

3. RESULTS AND DISCUSSION

3.1. Spectroscopic Characterization of the Precursor Complex

The synthesis of the precursor complex was easily accomplished at ambient conditions by simply mixing the metal salt and ligand and was found soluble only in DMSO. Actual. Yield: (1.45 g, 79%); White solid; m.p.: 194 °C; Anal. Cal. (Found), for $C_{10}H_{20}CdN_2S_4$: C, 29.37 (29.32), H, 4.93 (4.99), N, 6.85 (6.82), S, 31.36 (31.33)%. FT-IR (neat, cm^{-1}): 1483 (υ_{C-N}), 1004 (υ_{SCS}), 359 (υ_{Cd-S}). ^{1}H NMR ($CDCl_3$: δ (ppm), 300 MHz): 2.61–2.76 (4H, *q*, $J = 5.0$ Hz, N–CH_2), 0.89–0.90 (6H, *t*, $J = 5.1$ Hz, CH_3), ^{13}C-NMR (DMSO: δ (ppm), 75 MHz): 202.1 (CSS), 52.8 (–CH_2), 14.7 (–CH_3). The presence of bands, in the FT-IR spectra of the complex, at 359 cm^{-1} is assignable to Cd–S stretch[41,42] and a single peak for CS at 1004 cm^{-1} indicated the bidentate dithiocarbamate-Cd coordination.[43] Moreover, the band at 1483 cm^{-1} due to C–N stretch designates the partial double bond character, which arises due to resonance phenomena in the CNSS moiety upon complexation.[44,45] The assignment of the proton resonances was made by their peak multiplicity, intensity pattern and comparison of the integration values with the expected composition. The ^{1}H NMR spectrum of the complex exhibited a quartet for methylene protons (2.61–2.76 ppm) and triplet for methyl protons (0.89–0.90 ppm). The ^{13}C NMR spectrum showed an upfield shift of around 9 ppm in the SCS peak than the free ligand, which confirms ligand-metal coordination.[46] The remaining signals matched well with the expected values. Furthermore, the elemental composition (CHNS) of the compound was found in close agreement with the theoretically predicted composition, thus confirmed the clean synthesis of the precursor complex.

3.2. Structural Analysis and Formation Mechanism of CdS Nanostructures

To investigate the role of decomposing solvent and by-product as shape directing agents, FTIR analysis of both morphologies was undertaken (Fig. 1(c)). FT-IR spectra of both morphologies are closely similar and showing absorption peaks at 2918, 2929 cm^{-1} and 2854, 2845 cm^{-1} due to symmetric and asymmetric stretches of methylene group, while the stretching bands around 3430 and 3442 cm^{-1} are assigned to –NH_2 group and at 1591 and 1578 cm^{-1} to N–H bending vibrations. Moreover, the observed peaks at 1361, 1372, 1008, 996, 716 and 730 cm^{-1} is assignable to mixed stretching of N–C═S moiety[41] (Scheme 2). The FT-IR results indicate the presence of organic moiety with similar functional groups on the surface of both morphologies. On the basis of FT-IR results and molecular structure of the thermolysing solvents (en and OA) it can be assumed that the surface of CdS-NR is capped by *in situ* generated 3-(2-aminoethyl)-1,1-dibutylethiourea, while that of CdS-NS is capped by 1,1-diethyl-3-octylthiourea as both of these compounds contain similar functional groups. Thus, it can be inferred that different capping molecules (which have been formed by using different thermolysing solvent) have played a significant role in tuning the morphology of CdS. Previous reports showed that en as a thermolysing solvent assist in anisotropic growth resulting in nanorods.[47] In contrast, long chain organic amines have been found to be the most effective surfactant usually leads to the formation of small nanoparticles with spherical shape.[48]

Thermolysing the precursor complex in en resulted in the formation of nanorods with length between 23–44 nm

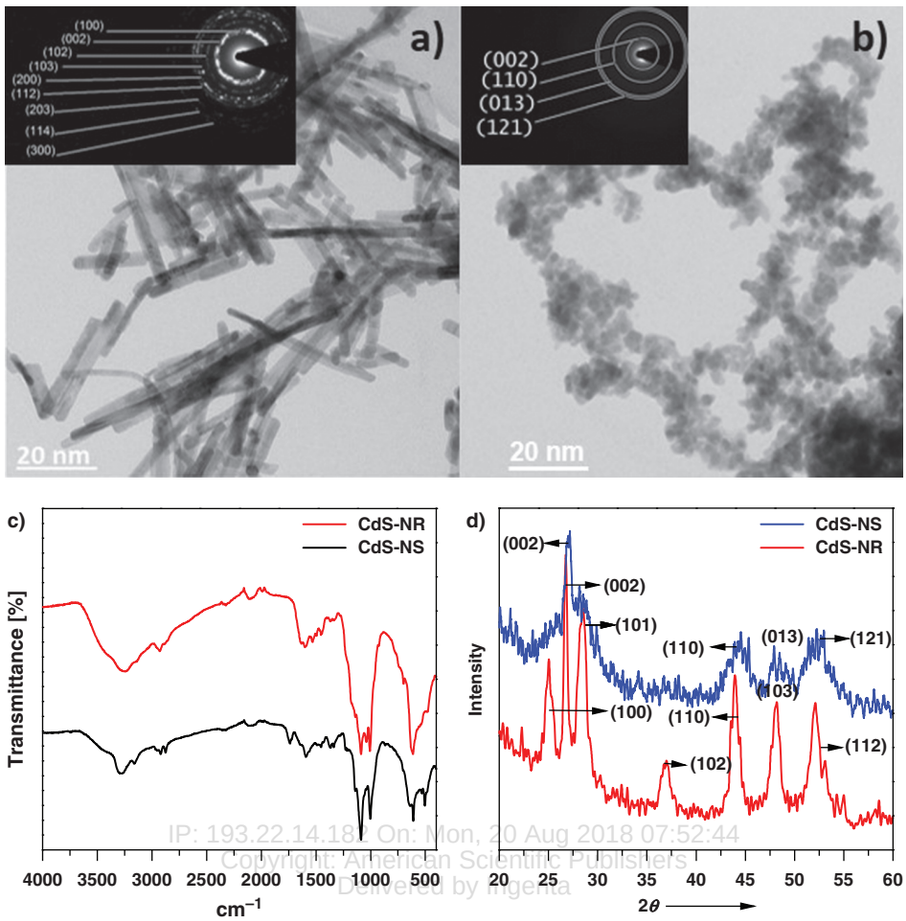

Figure 1. TEM images of (a) CdS-NR and its inset SAED pattern (b) CdS-NS and its inset SAED pattern (c) FTIR analysis and (d) PXRD diffraction of as-prepared CdS-NR and CdS-NS nanostructures.

and the diameter lie between 7–12 nm, however, in OA, it afforded nanospheres with size in the range of 2.89–5.30 nm as can be evidenced in the TEM images (Figs. 1(a, b)). The SAED pattern of CdS-NR and CdS-NS are shown in inset of Figures 1(a) and (b), respectively. The concentric circular fringes in the patterns revealed the polycrystalline nature of both morphologies. The calculated "*d*" values are 0.355, 0.334, 0.315, 0.244, 0.206, 0.188, 0.177 nm, which is in agreement with (100), (002), (102), (103), (112), (203) and (114) planes of CdS-NR and 0.3363, 0.2118, 0.1738 and 0.1419 nm agree to (002), (110), (013) and (121) "(*hkl*)" planes in case of CdS-NS. These results are in firm agreement with XRD patterns (Fig. 1(d)) of both morphologies. The diffraction peaks of CdS-NR can be indexed to the hexagonal CdS with lattice constants $a = b = 4.12$ Å and $c = 6.63$ Å, which correspond to *ICSD* file [01-080-0006] hexagonal structure having space group *(P63mc)*. These prominent peaks correspond to the reflections at $2\theta = 25.04°$ (100), 26.68° (002), 28.30° (101), 36.83° (102), 43.94 (110), 48.17° (103) and 52.11° (112). Compared to the standard *ICSD* file the highly intense peak at 26.68° with a *d*-spacing value of 0.334 nm can be assigned to the (002) plane which reveals the oriented growth of the hexagonal CdS along *c*-axis, a clear indication of nanorod morphology.[39, 49] The absence of extra peaks beside the reflections from CdS, ruled out the possibilities of any other impurity. Similarly, the diffraction peaks of CdS-NS are indexed as the Cubic mixed hexagonal CdS which correspond to *ICSD* file [00-001-0647] having space group (*F-43m*). The XRD spectrum of CdS-NS (Fig. 1(d)), apparently exhibited only four broad peaks, centered at $2\theta = 27.15°$ (002), 44.50° (110), 48.16° (013) and 52.31° (121). On close observation, the broad peak at 27.15° was found to have been originated by the overlap of shoulders on both the sides at $2\theta = 24°$ and 28° (resulting from the overlap of reflections from (100), (002) and (101) planes) of the hexagonal W-type structure.[50] The peaks broadening and overlapping can be attributed to the smaller size of the CdS-NS, which can also be evidenced in the TEM results. Moreover, the three most prominent peaks for cubic CdS with Z-type structure occur at 27.15° (111), 44.50° (220) and 52.31° (311) reveal the existence of cubic CdS and could not be ruled out based

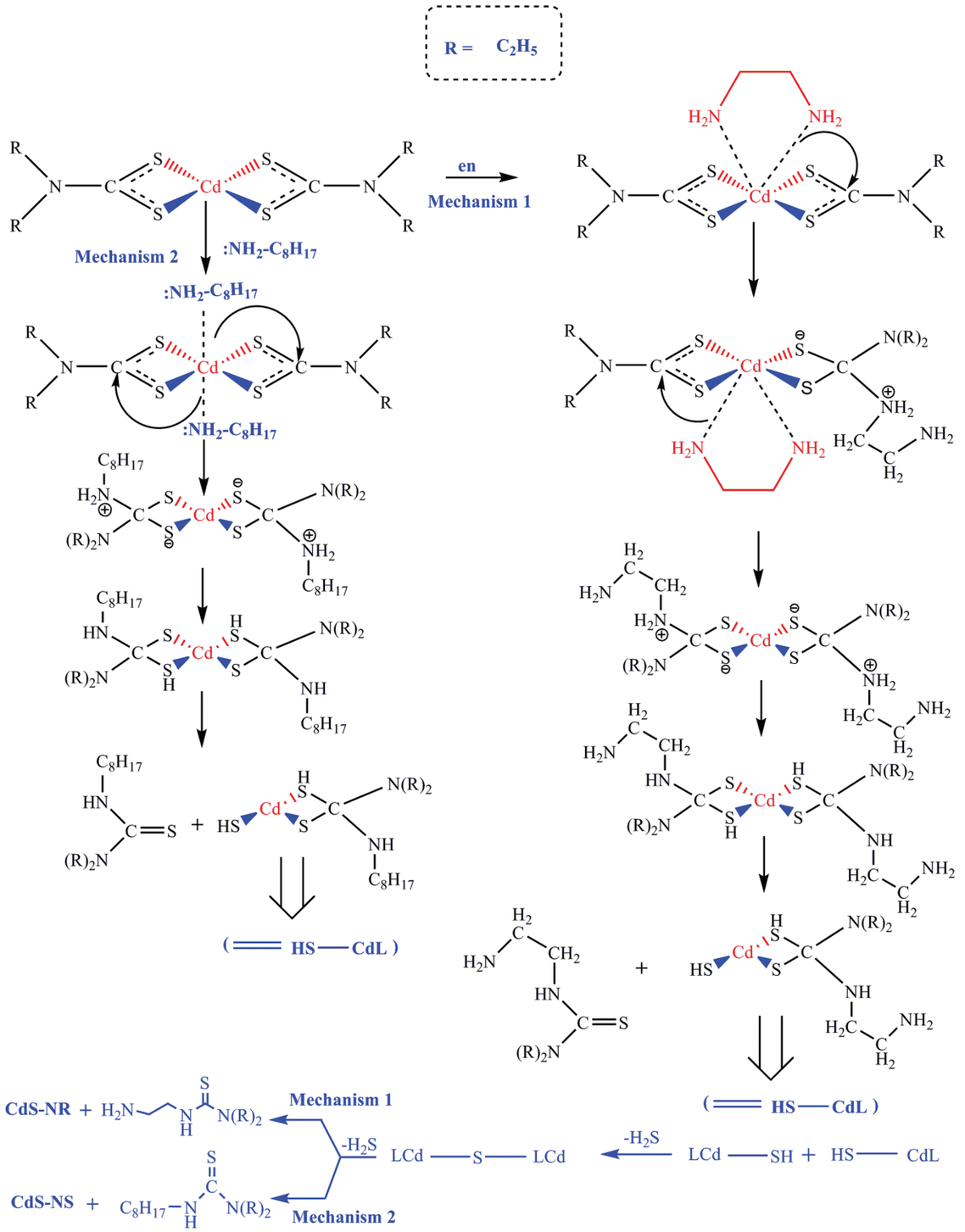

Scheme 2. Mechanism for the preparation of CdS-NR and CdS-NS in the presence of en (mechanism 1) and OA (mechanism 2), respectively.

on XRD information, which suggest that CdS-NS possesses prominent features of both phases and had a distorted structure resulting due to the fractional contents of both the phases.[51, 52] The Energy-dispersive X-ray Spectroscopy (EDS) spectra of the synthesized CdS-NR and CdS-NS measurements confirmed the presence of Cd and S in 1:1 stoichiometric ratio. The peaks due to carbon, aluminum, oxygen, zirconium and bromine were because of sputter coating of the glass substrate on the EDS stage and were not taken into consideration.

3.3. Optical Property

To assess the optical properties of the synthesized materials, UV-visible and PL spectroscopy was undertaken. As shown in Figure 2(a) the absorption maxima of CdS-NR appears at 480 nm and CdS-NS at 470 nm which corresponds to the band gap of 2.58 eV and 2.63 eV, respectively. The band gap energy of both morphologies suggests their photocatalytic potential in the visible region. The photoluminesce (PL) spectrum of CdS-NR and CdS-NS is shown in Figure 2(b). The decrease in PL intensity in the case of CdS-NR can be attributed to the spatial anisotropic effect of the optical dipole emission of NR. The effect of such emission from nanocrystals is expected to be maximum in the plane perpendicular to the dipole and minimum when it is along the direction of nanorod axis. Moreover, the time decay curve in the case of CdS-NR clearly indicated enough long lifetime for electron–hole pairs and suppression of charge recombination rate (Fig. 2(c)).

3.4. Photocatalytic Activity

To assess the solar light assisted photocatalytic potential of both morphologies, a CR dye degradation was carried out as a model reaction. The progress of degradation was inspected with time interval of 3 minutes by observing the decrease in absorption intensity of azo (497 nm) and naphthalene (338 nm) groups. As shown in Figures 3(a) and (b), the degradation of CR dye on CdS-NR is relatively fast (21 min.) than CdS-NS (27 min.). On CdS-NR, both azo and aromatic ring were degraded more efficiently (98% and 94%) than that of CdS-NS (95% and 91%). The linear relationship of $\ln(C_i/C_0)$ versus time (min) indicated that both photocatalysts followed pseudo-fist-order kinetics (Fig. 3(c)). The obtained rate constant expression is represented by the following equation (Eq. (1))[53]

$$\ln(C_i/C_0) = k_{app}t \quad (1)$$

Where k_{app} is the rate constant and C_i and C_0 are the initial and final concentrations of CR, respectively. The CdS-NR ($k_{app} = 0.366$ min^{-1}) shows high photocatalytic activity than CdS-NS ($k_{app} = 0.299$ min^{-1}). The degradation percentile for CdS-NR and CdS-NS were found more than 98% and 96%, respectively (Fig. 3(d)).

To study the effect of catalyst dose, the catalyst amount was varied for the constant amount of CR dye. It was observed that rate constant was gradually increased with increasing catalyst dose (4 mg to 24 mg) (Fig. 3(e)). This is due to an increase in the number of available catalyst particles, which in turns increases the number of active sites, thus enhances the adsorption of CR molecules and high photons trapping required for degradation.[54,55] The photocatalytic behavior of CdS-NR and CdS-NS was confirmed by no CR degradation in the absence of NPs, though solar light was available. Moreover, no significant activity was observed in the dark despite the presence of catalysts for almost 8 hours, which further confirm that degradation process is only photocatalytically driven i.e., both light and catalyst are required.

3.5. Stability and Reusability of CdS Nanostructures

To check the stability and reusability of CdS-NR and CdS-NS, the five-time recycling process was carried out for both catalysts under the similar experimental conditions (Fig. 3(f)). The stability constant $K_{app} = 0.261$ min^{-1} (CdS-NR) and 0.229 min^{-1} (CdS-NS) was calculated in the fifth cycle. Furthermore, the catalyst materials collected after fifth cycle were dispersed in aqueous media and subjected to UV-visible absorption analysis to examine any shift in the absorption maximum (λ_{max}). The red shift in absorption spectrum of CdS-NS was observed to be more significant, an indication of particles aggregation during photo degradation.[54] Commensurate with this analysis, we have observed a slight decrease in the catalytic activity after each cycle. This might be due to run off the catalyst material during filtering and washing. Importantly, we have not detected any significant concentration of leached Cd^{2+} ion {detection limit ≥ 3 μg/L (0.003 ppm)} when titrated the degraded dye solution containing CdS particles (200 mg/L) against EDTA (0.1 M) as titrant and erichrome black-t (0.2 g in 15 mL) as indicator at pH of 6.5–7.[56]

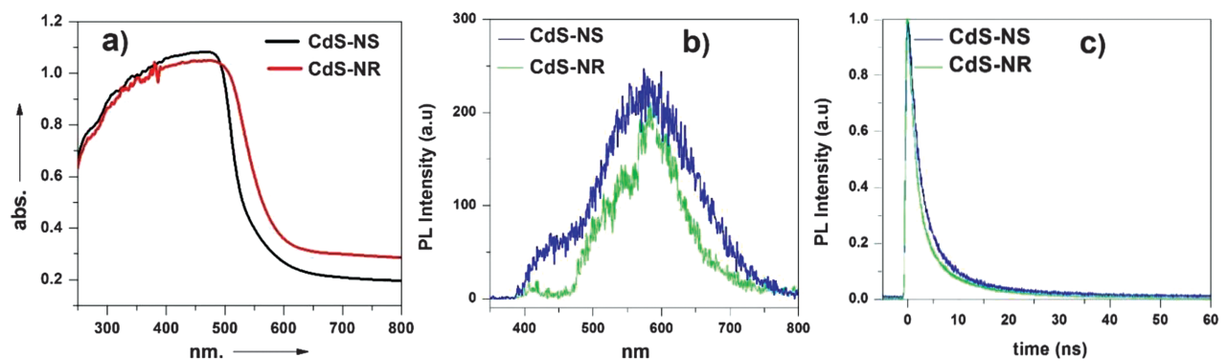

Figure 2. (a) UV-visible absorption spectra (b) steady-state photoluminescence (PL) and (c) time-resolved of as-prepared CdS nanostructures.

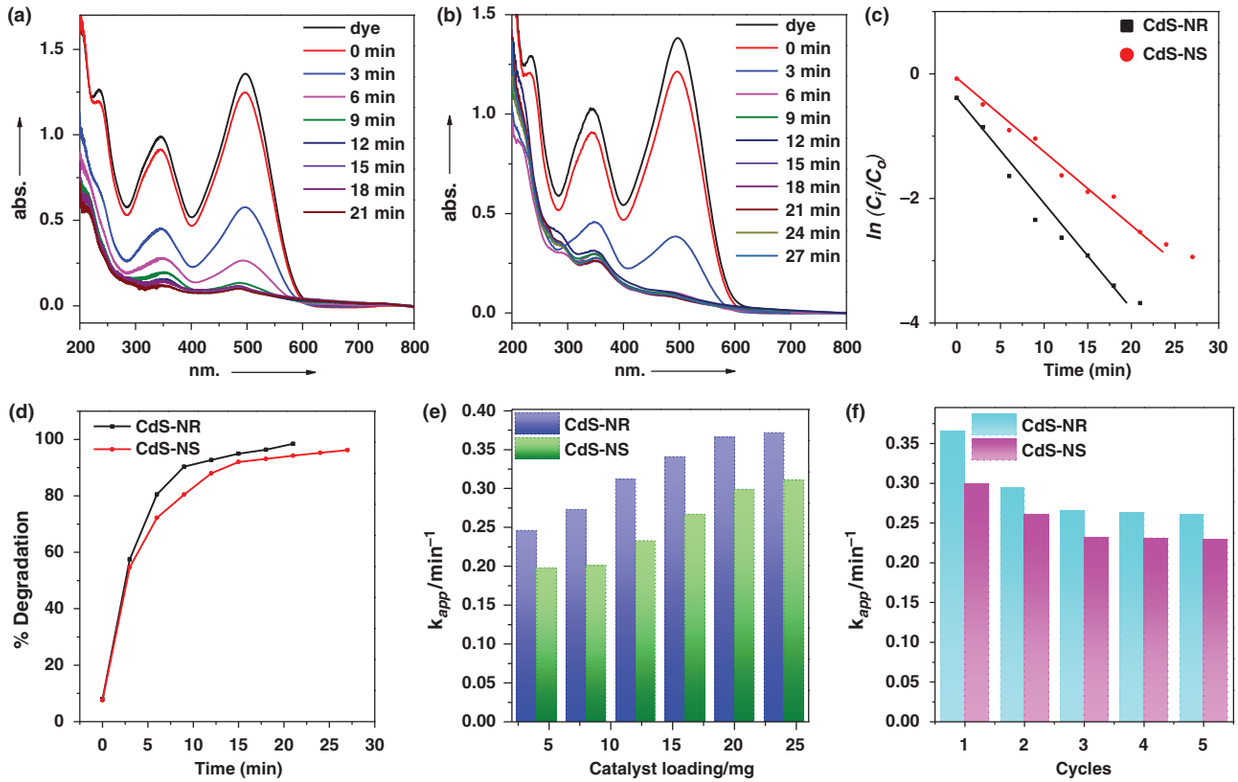

Figure 3. UV-visible absorption spectra of successive CR degradation in the presence of (a) CdS-NR (b) and CdS-NS (c) the plot $\ln(C_i/C_0)$ versus reaction time (min^{-1}) (d) % degradation plot (e) effect of catalysts loading and (f) the recycling stability of the synthesized CdS-NR and CdS-NS.

In view of above results and some previous reports, the nanorod morphology exhibited better photocatalytic activity as compared to other morphologies. A relatively longer life time of electron–hole pair and suppression of recombination phenomenon was observed in case of rod-like morphology, as evident from the PL results. This is because the charge carriers transport in case of the nanorod is well channelized which in turn suppresses the recombination process.[40] Furthermore, low photocatalytic efficiency of CdS-NS despite of its smaller NPs size than the Cd-NR, may be due to high particles merging of the fomer that may in turn decrease the quantum efficiency.

3.6. Photocatalytic Mechanism

A proposed mechanism on the basis of above-mentioned results is explained as follow: Irradiation of light on the surface of photocatalyst leads to the formation of electron–hole pairs when the photon energy equal to or exceeds the band gap energy of semiconductor (Fig. 4) (step 1). The main protagonist behind the degradation of CR dye are O_2^- ion and ·OH radicals. The ·O_2^- ion is formed when photoinduced electron reduces the molecular oxygen.[54] While the highly reactive ·OH radical is generated by two different pathways. In one of the path way, photogenerated holes (h^+) is captured by a hydroxyl group and produce highly reactive hydroxyl radicals (·OH) (Step 2 and 3) and H_2O. On the other hand, a photoinduced electron reduces the adsorbed molecular oxygen (O_2) to the oxygen radical (superoxide radical anion/·O_2^-) (Step 4)[54] which is then further oxidized by hole and generate $HO_2^{\cdot}$ radical (5). The highly reactive $HO_2^{\cdot}$ radicals combine and produce H_2O_2 molecule (Step 6) which is further reduced by electron and

$$CdS + h\nu \longrightarrow h^+ + e^- \quad 1)$$
$$h^+ + OH^- \longrightarrow {}^{\cdot}OH \quad 2)$$
$$h^+ + H_2O \longrightarrow {}^{\cdot}OH \quad 3)$$
$$O_2 + e^- \longrightarrow {}^{\cdot}O_2^- \quad 4)$$
$${}^{\cdot}O_2^- + H^+ \longrightarrow HO_2^{\cdot} \quad 5)$$
$$2HO_2^{\cdot} \longrightarrow O_2 + H_2O_2 \quad 6)$$
$$H_2O_2 + e^- \longrightarrow {}^{\cdot}OH + {}^-OH \quad 7)$$
$$H_2O_2 + O_2 \longrightarrow {}^{\cdot}OH + {}^-OH + O_2 \quad 8)$$
$${}^{\cdot}O_2^-/{}^{\cdot}OH + dye \longrightarrow Degrade + Product \quad 9)$$

Figure 4. The proposed mechanism for the degradation of Congo Red (CR) dye on CdS nanostructures.

generate $^{\bullet}OH$ and ^{-}OH (step 7). Furthermore, the molecular H_2O_2 is also split into $^{\bullet}OH$ radical and ^{-}OH ion in the presence of oxygen (step 8). These two highly reactive species $^{\bullet}O_2^-$ and $^{\bullet}OH$ are the main driven forces behind the effective decomposition of CR dye (Step 9). Moreover, $^{\bullet}O_2^-$, $^{\bullet}OH$ and $HO_2^{\bullet}$ are the three main reactive intermediates in the whole process.

4. CONCLUSION

In summary, synthesis and conversion of the precursor complex to CdS nanostructures were easily achieved under mild conditions using en and OA as thermolysing solvents. Two different morphologies nanorods (en) and nanosphers (OA) were obtained as confirmed by TEM analysis. The morphological effect of solvent can be attributed to the role of different *in situ* generated capping ligands, as confirmed by FT-IR analysis. Furthermore, the XRD results revealed the growth of nanorods into hexagonal while the nanospheres into cubic mixed hexagonal phase. Both morphologies absorb in the visible region (UV/visible absorption spectroscopy), thus have the ability to be used as solar light driven photocatalysts. However, the decrease in PL and time decay curve have confirmed the low electron–hole recombination of NR than NS, thus signified the better photocatalytic potential of the former. This fact was further confirmed by efficient solar light assisted degradation of CR on CdS-NR ($k_{app} = 0.366$ min^{-1}) than CdS-NS ($k_{app} = 0.299$ min^{-1}). Furthermore, both CdS-NR and CdS-NS are stable enough to be used in multiple cycle without compromising on the efficiency. So prolonging electron–hole recombination time by morphological tuning through a facile procedure may be a cost effective approach for harvesting solar light for the purpose of energy and environmental stability.

Disclosure Statement

We have no potential conflict of interest.

Acknowledgments: We acknowledge the financial support from the Higher education Commission (HEC) of Pakistan and International Joint Project of Hainan Province (grant no. ZDYF2016212).

References and Notes

1. E. Forgacs, T. Cserhati, and G. Oros, *Environ. Int.* 30, 953 **(2004)**.
2. E. Abadulla, T. Tzanov, S. Costa, K.-H. Robra, A. Cavaco-Paulo, and G. M. Gübitz, *Appl. Environ. Microbiol.* 66, 3357 **(2000)**.
3. N. Daneshvar, A. Oladegaragoze, and N. Djafarzadeh, *J. Hazard. Mater.* 129, 116 **(2006)**.
4. S. Senthilkumaar, P. Varadarajan, K. Porkodi, and C. Subbhuraam, *J. Colloid Interface Sci.* 284, 78 **(2005)**.
5. M. H. Habibi, A. Hassanzadeh, and S. Mahdavi, *J. Photochem. Photobiol.* 172, 89 **(2005)**.
6. T. E. Agustina, H. Ang, and V. Vareek, *J. Photochem. Photobiol. C: Photochemistry Reviews* 6, 264 **(2005)**.
7. D. Kavitha and C. Namasivayam, *Bioresource Technology* 98, 14 **(2007)**.
8. J. Wu, M. A. Eiteman, and S. E. Law, *J. Environ. Eng.* 124, 272 **(1998)**.
9. P. C. Vandevivere, R. Bianchi, and W. Verstraete, *J. Chem. Technol. Biotechnol.* 72, 289 **(1998)**.
10. W. Liu, *Mater. Lett.* 60, 551 **(2006)**.
11. K. Kandasamy, H. B. Singh, and S. K. Kulshreshtha, *J. Chem. Sci.* 121, 293 **(2009)**.
12. H. Zhu, R. Jiang, L. Xiao, Y. Chang, Y. Guan, X. Li, and G. Zeng, *J. Hazard. Mater.* 169, 933 **(2009)**.
13. D. S. Bhatkhande, V. G. Pangarkar, and A. A. Beenackers, *J. Chem. Technol. Biotechnol.* 77, 102 **(2002)**.
14. W. Lei, D. Portehault, D. Liu, S. Qin, and Y. Chen, *Nat. Commun.* 4, 1777 **(2013)**.
15. G. Madhusudana, P. S. Kumar, D. P. Kumar, V. V. Srikanth, and M. V. Shankar, *Mater. Lett.* 128, 183 **(2014)**.
16. D. Kumar and M. Kumari, *ChemComm.* 49, 9443 **(2013)**.
17. H. Tang, D. Zhang, G. Tang, X. Ji, C. Li, X. Yan, and Q. Wu, *J. Alloys Compd.* 591, 52 **(2014)**.
18. Y. Liu, Y. Jiao, Z. Zhang, F. Qu, A. Umar, and X. Wu, *ACS Appl. Mater. Interfaces* 6, 2174 **(2014)**.
19. C. Karunakaran, S. S. Raadha, and P. Gomathisankar, *J. Alloys Compd.* 549, 269 **(2013)**.
20. X. Li, X. Lu, Y. Meng, C. Yao, and Z. Chen, *J. Alloys Compd.* 562, 56 **(2013)**.
21. M. Shankar, S. Nélieu, L. Kerhoas, and J. Einhorn, *Chemosphere* 66, 767 **(2007)**.
22. C. Han, L. Ge, C. Chen, Y. Li, X. Xiao, Y. Zhang, and L. Guo, *Appl. Catal. B* 147, 546 **(2014)**.
23. S. Shi, M. Gondal, A. Al-Saadi, R. Fajgar, J. Kupcik, X. Chang, K. Shen, Q. Xu, and Z. Seddigi, *J. Colloid Interface Sci.* 416, 212 **(2014)**.
24. J. Wang, B. Li, J. Chen, N. Li, J. Zheng, J. Zhao, and Z. Zhu, *J. Alloys Compd.* 535, 15 **(2012)**.
25. S. Peng, L. Li, Y. Wu, L. Jia, L. Tian, M. Srinivasan, S. Ramakrishna, Q. Yan, and S. G. Mhaisalkar, *CrystEngComm.* 15, 1922 **(2013)**.
26. X. Meng, G. Tian, Y. Chen, R. Zhai, J. Zhou, Y. Shi, X. Cao, W. Zhou, and H. Fu, *CrystEngComm.* 15, 5144 **(2013)**.
27. M. Muruganandham, R. Amutha, E. Repo, M. Sillanpää, Y. Kusumoto, and M. Abdulla-Al-Mamun, *J. Photochem. Photobiol. A: Chemistry* 216, 133 **(2010)**.
28. A. Ajmal, I. Majeed, R. N. Malik, H. Idriss, and M. A. Nadeem, *RSC Adv.* 4, 37003 **(2014)**.
29. S. Kaur and V. Singh, *J. Hazard. Mater.* 141, 230 **(2007)**.
30. S. Chakrabarti and B. K. Dutta, *J. Hazard. Mater.* 112, 269 **(2004)**.
31. H. R. Pouretedal, A. Norozi, M. H. Keshavarz, and A. Semnani, *J. Hazard. Mater.* 162, 674 **(2009)**.
32. J. Yu, Y. Yu, P. Zhou, W. Xiao, and B. Cheng, *Appl. Catal. B* 156, 184 **(2014)**.
33. Z. Yu, B. Yin, F. Qu, and X. Wu, *Chem. Eng. J.* 258, 203 **(2014)**.
34. N. Bao, L. Shen, T. Takata, and K. Domen, *Chem. Mater.* 20, 110 **(2007)**.
35. C. Li, L. Han, R. Liu, H. Li, S. Zhang, and G. Zhang, *J. Mater. Chem.* 22, 23815 **(2012)**.
36. L. Shen, N. Bao, P. E. Prevelige, and A. Gupta, *J. Phys. Chem. C* 114, 2551 **(2010)**.
37. D. Jing and L. Guo, *J. Phys. Chem. B* 110, 11139 **(2006)**.
38. M. Muruganandham, Y. Kusumoto, C. Okamoto, A. Muruganandham, M. Abdulla-Al-Mamun, and B. Ahmmad, *J. Phys. Chem. C* 113, 19506 **(2009)**.
39. J. Yu, Y. Yu, and B. Cheng, *RSC Adv.* 2, 11829 **(2012)**.
40. A. Khan, Zia-ur-Rehman, A. Khan, H. Ambareen, H. Ullah, S. M. Abbas, Y. Khan, and R. Khan, *Inorg. Chem. Commun.* 79, 99 **(2017)**.
41. A. Khan, Zia-ur-Rehman, Muneeb-ur-Rehman, R. Khan, A. Waseem, A. Iqbal, and Z. H. Shah, *Inorg. Chem. Commun.* 72, 33 **(2016)**.
42. E. D. Risberg, J. Mink, A. Abbasi, M. Y. Skripkin, L. Hajba, P. Lindqvist-Reis, and M. Sandström, *Dalton Trans.* 8, 1328 **(2009)**.

43. F. Shaheen, A. Badshah, M. Gielen, G. Croce, U. Florke, D. de Vos, and S. Ali, *J. Organomet. Chem.* 695, 315 **(2010)**.
44. N. Thammakan and E. Somsook, *Mater. Lett.* 60, 1161 **(2006)**.
45. M. K. Amir, Zia-ur-Rehman, F. Hayat, S. Z. Khan, G. Hogarth, T. Kondratyuk, J. M. Pezzuto, and M. N. Tahir, *RSC Adv.* 6, 110517 **(2016)**.
46. S. Z. Khan, M. K. Amir, I. Ullah, A. Aamir, J. M. Pezzuto, T. Kondratyuk, F. Bélanger-Gariepy, A. Ali, S. Khan, and Zia-ur-Rehman, *Appl. Organomet. Chem.* 30, 392 **(2016)**.
47. B. Zhang, W. Yao, C. Huang, Q. Xu, and Q. Wu, *Int. J. Hydrogen Energy* 38, 7224 **(2013)**.
48. Z. Zhang, W. P. Lim, C. T. Wong, H. Xu, F. Yin, and W. S. Chin, *Nanomaterials* 2, 113 **(2012)**.
49. H. Zhang, X. Ma, Y. Ji, J. Xu, and D. Yang, *Chem. Phys. Lett.* 377, 654 **(2003)**.
50. P. Christian and P. O'Brien, *J. Mater. Chem.* 18, 1689 **(2008)**.
51. R. Banerjee, R. Jayakrishnan, and P. Ayyub, *J. Phys. Condens. Matter* 12, 10647 **(2000)**.
52. A. Vorokh and A. Rempel, *Phys. Solid State* 49, 148 **(2007)**.
53. S. Lan, L. Liu, R. Li, Z. Leng, and S. Gan, *Ind. Eng. Chem. Res.* 53, 3131 **(2014)**.
54. H. Zhu, R. Jiang, L. Xiao, Y. Chang, Y. Guan, X. Li, and G. Zeng, *J. Hazard. Mater.* 169, 933 **(2009)**.
55. V. A. Sakkas, M. A. Islam, C. Stalikas, and T. A. Albanis, *J. Hazard. Mater.* 175, 33 **(2010)**.
56. M. Jawaid, *Talanta* 27, 95 **(1980)**.

Received: 1 February 2018. Accepted: 26 March 2018.